Inorganic Chemistry

Article

pubs.acs.org/IC

Thermal Response, Catalytic Activity, and Color Change of the First Hybrid Vanadate Containing Bpe Guest Molecules

Roberto Fernández de Luis,[†] M. Karmele Urtiaga,[†] José L. Mesa,[‡] Edurne S. Larrea,[†] Marta Iglesias,[§] Teófilo Rojo,[‡] and María I. Arriortua*[,†]

[†]Departamento de Mineralogía y Petrología and [‡]Departamento de Química Inorgánica, Facultad de Ciencia y Tecnología, Universidad del País Vasco, UPV/EHU, Apdo. 644, E-48080 Bilbao, Spain

[§]Instituto de Ciencia de Materiales de Madrid-CSIC, Sor Juana Inés de la Cruz 3, Cantoblanco, 28049 Madrid, Spain

Supporting Information

ABSTRACT: Four isomorphic compounds with formula $[\{Co_2(H_2O)_2(Bpe)_2\}(V_4O_{12})]\cdot 4H_2O\cdot Bpe$, CoBpe **1**; $[\{CoNi(H_2O)_2(Bpe)_2\}(V_4O_{12})]\cdot 4H_2O\cdot Bpe$, CoNiBpe **2**; $[\{Co_{0.6}Ni_{1.4}(H_2O)_2(Bpe)_2\}(V_4O_{12})]\cdot 4H_2O\cdot Bpe$, NiCoBpe **3**; and $[\{Ni_2(H_2O)_2(Bpe)_2\}(V_4O_{12})]\cdot 4H_2O\cdot Bpe$, NiBpe **4**, have been obtained by hydrothermal synthesis. The crystal structures of CoBpe **1** and NiBpe **4** were determined by single-crystal X-ray diffraction (XRD). The Rietveld refinement of CoNiBpe **2** and NiCoBpe **3** XRD patterns confirms that those are isomorphic. The compounds crystallize in the $P\bar{1}$ space group, exhibiting a crystal structure constructed from inorganic layers pillared by Bpe ligands. The crystal structure contains intralayer and interlayer channels, in which the crystallization water molecules and Bpe guest molecules, respectively, are located. The solvent molecules establish a hydrogen bonding network with the coordinated water molecules. Thermodiffractometric and thermogravimetric studies showed that the loss of crystallization and coordinated water molecules takes place at different temperatures, giving rise to crystal structure transformations that involve important reduction of the interlayer distance, and strong reduction of crystallinity. The IR, Raman, and UV−vis spectra of the as-synthesized and heated compounds confirm that the structural building blocks and octahedral coordination environment of the metal centers are maintained after the structural transformations. The color change and reversibility of the water molecules uptake/removal were tested showing that the initial color is not completely recovered when the compounds are heated at temperatures higher than 200 °C. The thermal evolution of the magnetic susceptibility indicates one-dimensional antiferromagnetic coupling of the metal centers at high temperatures. For NiCoBpe **3** and NiBpe **4** compounds magnetic ordering is established at low temperatures, as can be judged by the maxima observed in the magnetic susceptibilities. CoNiBpe **2** was proved as catalyst being active for cyanosilylation reactions of aldehydes.

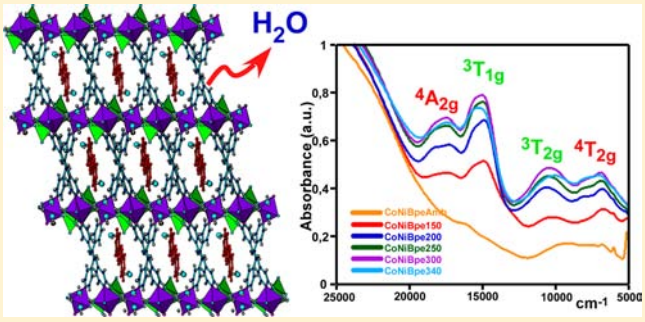

INTRODUCTION

Hybrid inorganic−organic materials have become a major research topic in material science, because of their ability to exhibit functionality from both the inorganic and organic components.[1] The combination of inorganic building blocks with rationally designed or functionalized organic ligands,[2] which could act as direct pillars of the crystal frameworks,[3] or as countercations balancing the charge of the anionic scaffold,[4] have given rise to amazing combined properties such as guest dependent spin cross over, net polarization and ferroelectricity, and electronic and photoactive metal−organic frameworks.[5] This type of material has great potential applications in many fields, such as catalysis,[6] medicine, sorption, electronic and ionic conductivity,[7] magnetism and photochemistry, among others.[8]

One prolific subclass of inorganic−organic hybrid materials is characterized by the incorporation of metal−organic complexes and vanadium oxide moieties into a single structure.[9] Hybrid vanadates with first-row transition metals exhibit very rich crystal chemistry, with several structural archetypes according to the metal center, the geometry of the ligand, and the different vanadium oxide subunits, such as clusters, rings, chains, layers, and three-dimensional frameworks.[10] The polymer grade is closely related to the synthetic conditions and, in particular, to the pH during the reaction.[11] The choice of the organic ligand is determinant for the structure of the resulting vanadates. Depending on the number of donor atoms, their relative positions to each other and the flexibility of the ligand, it could act chelating a metal center or bridging two metal atoms. This fact conditions the structure and, hence, the properties of the material.[12] In that regard, the thermal stability and thermal response of the crystal structure to the loss of guest molecules and/or coordinated species is intimately related with the crystal framework itself and more specifically with the

Received: December 5, 2012
Published: February 14, 2013

   dx.doi.org/10.1021/ic302662x | Inorg. Chem. 2013, 52, 2615−2626

combination of rigid or flexible inorganic and metal organic subnets within the hybrid vanadate crystal structure. For example, the rigid three-dimensional inorganic scaffolds stabilized by rigid organic pillars in $[\{Ni_6(H_2O)_{10}(Bpy)_6\}V_{18}O_{51}]\cdot 1.5H_2O$ and $[\{Ni(H_2O)_2(Bpe)\}V_4O_{11}]\cdot 0.5H_2O$ give rise to an irreversible loss of coordinated water molecules with a drastic reduction of the crystallinity during the process and practically no changes associated with the removal of crystallization water molecules.[13] The crystal structures of $[\{Mn(Bpy)\}(VO_3)_2]\cdot(H_2O)_{1.16}$ and $[\{Mn(Bpy)_{0.5}\}(VO_3)_2]\cdot(H_2O)_{0.62}$ exhibit dynamic and reversible responses to the loss/uptake of crystallization water molecules.[14] Intermediate behaviors are observed in $[\{Ni_8(Bpy)_{16}\}V_{24}O_{68}]\cdot 8.5(H_2O)$ and $[\{Ni_3(H_2O)_3(Bpa)_4\}(V_6O_{18})]\cdot 8H_2O$, because of the combination of both three-dimensional metal−organic and inorganic scaffolds in the same crystal architectures.[15] The dynamic and reversible single crystal to single crystal transformation due to the removal/addition of coordinated water molecules in $[Co_2(ppca)_2(H_2O)(V_4O_{12})_{0.5}]$ generates changes in the coordination environment of the Co(II) metal centers and hence to an appreciable change in the sample color.[16] The variation of the coordination environment of the metal centers could give rise to interesting changes in the physical properties such as color, leading to materials with potential applications in sensing devices. Moreover, the existence of coordinated unsaturated metal sites is very beneficial in porous materials, providing Lewis acid sites in the structure, usable for the surface post- functionalization for specific catalytic reactions.[17]

Heterogeneous catalysis is a vital component of the chemical industry, and it is involved to some degree in 90% of the chemical manufacturing processes currently in use.[18] The main advantage of using heterogeneous catalysts is their facile recovering and recycling. As far as we are concerned, the first study of catalytic properties of hybrid vanadates was made in our research group over a family of compounds with the formula $M(HAep)_2(VO_3)_4$, where M = Co(II), Ni(II), and Cu(II).[19] These compounds act as heterogeneous catalysts for the selective oxidation of alkyl aryl sulfides, with both H_2O_2 and *tert*-butylhydroperoxide as oxidizing agents.

Herein, here we report four isomorphic materials with formulas $[\{Co_2(H_2O)_2(Bpe)_2\}(V_4O_{12})]\cdot 4H_2O\cdot Bpe$, CoBpe **1**; $[\{CoNi(H_2O)_2(Bpe)_2\}(V_4O_{12})]\cdot 4H_2O\cdot Bpe$, CoNiBpe **2**; $[\{Co_{0.6}Ni_{1.4}(H_2O)_2(Bpe)_2\}(V_4O_{12})]\cdot 4H_2O\cdot Bpe$, NiCoBpe **3**; and $[\{Ni_2(H_2O)_2(Bpe)_2\}(V_4O_{12})]\cdot 4H_2O\cdot Bpe$, NiBpe **4** have been obtained by hydrothermal synthesis. Hereafter, the acronyms CoBpe **1**, CoNiBpe **2**, NiCoBpe **3**, and CoBpe **4** are used in the discussion of the crystal structures, thermal, spectroscopic, magnetic, and catalytic properties of these materials. The crystalline to pseudoamorphous transformations associated with the reversible loss/uptake of crystallization and coordinated water molecules, and the reversibility of the color change related to these processes are also studied. Moreover, the high yield of the hydrothermal reaction for the CoNiBpe **2** compound has allowed obtaining enough quantity of material to carry out UV−vis spectra after heating the compound at different temperatures and to test the catalytic activity of the material for the cyanosilylation reaction of aldehydes.

EXPERIMENTAL SECTION

Materials and Methods. Commercially available reagent grade chemicals were purchased from Sigma-Aldrich. These were used without further purification. All synthetic reactions were carried out in 50 mL Parr Teflon-lined acid digestion bombs. The same synthesis pathway was used to prepare all the studied compounds. The reagents were mixed in 30 mL of distilled water under vigorous stirring. The pH value was adjusted with 1 M HNO_3 solution. The mixtures were placed in 50-mL Parr Teflon lined autoclaves and heated at 120 °C for 3 days in an electric furnace. After the reaction was complete, the products were washed with distilled water and acetone, dried in air, and observed under a binocular microscope. In all the studied hydrothermal conditions the synthesized compounds cocrystallize with other hybrid vanadates. In order to obtain pure samples, the manual separation of the single-crystals was carried out under a binocular microscope.

Synthesis of CoBpe 1. Reagents: $Co(NO_3)_2\cdot 6H_2O$ (0.52 mmol), $NaVO_3$ (1.04 mmol), Bpe (1.04 mmol), H_2O (30 mL), pH value: 6.5. After the reaction brown prism single crystals of CoBpe **1** together with an uncharacterized yellow hybrid vanadate were obtained. CoBpe **1** compound is a minor product of the hydrothermal reaction. After the manual separation approximately 2 mg of sample per reaction are obtained.

Synthesis of CoNiBpe 2. Reagents: $Co(NO_3)_2\cdot 6H_2O$ (0.13 mmol), $Ni(NO_3)_2\cdot 6H_2O$ (0.13 mmol), $NaVO_3$ (0.26 mmol), Bpe (0.26 mmol), H_2O (30 mL), pH value: 6.0. After the reaction orange prism single crystals of CoNiBpe **2** together with dark brown single-crystals of $\{Co_{0.5}Ni_{0.5}(Bpe)\}(VO_3)_2$ compound were obtained. That compound is isomorphic unit previously reported $\{Ni(Bpe)\}(VO_3)_2$ phase [see ref 12c].

Synthesis of NiCoBpe 3. Reagents: $Co(NO_3)_2\cdot 6H_2O$ (0.078 mmol), $Ni(NO_3)_2\cdot 6H_2O$ (0.182 mmol), $NaVO_3$ (0.26 mmol), Bpe (0.26 mmol), H_2O (30 mL), pH value: 6.0. After the reaction orange prism single crystals of NiCoBpe **3** together with dark brown single crystals of $\{Co_{0.3}Ni_{0.7}(Bpe)\}(VO_3)_2$ compound were obtained. That compound is isomorphic with previously reported $\{Ni(Bpe)\}(VO_3)_2$ phase [see ref 12c].

Synthesis of NiBpe 4. Reagents: $Ni(NO_3)_2\cdot 6H_2O$ (0.26 mmol), $NaVO_3$ (0.26 mmol), Bpe (0.52 mmol), H_2O (30 mLb X-ray diffraction patterns of as-synthesized CoNiBpe **2** compound and recycled CoNiBpe **2** after the cyanosilylation reactions), pH value: 6.5. After the reaction pale green prism single-crystals of NiBpe **4** together with emerald green single crystals of $\{Ni(Bpe)\}(VO_3)_2$ compound were obtained [see ref 12c]. The NiBpe **4** compound is a minor phase of the hydrothermal reaction. After the manual separation of the single crystals approximately 4 mg of sample per reaction are obtained.

The samples were characterized by X-ray powder diffraction data, recorded in a BRUKER D8 ADVANCE Vário diffractometer (CuKα1 radiation, 2θ range = 5−70°, step size = 0.015°, exposure time = 10 s per step). The final result of the Rietveld refinement with a fixed structural model confirms that the compounds are isomorphic and the inexistence of impurities. For NiBpe **4** a pattern matching analysis instead of a Rietveld refinement was carried out due to the strong preference orientation of the (010) family planes. (CoBpe **1**: $\chi^2 = 2.42$, $R_B = 21.5$, $R_p = 17.2$, $R_{wp} = 23.0$, $R_{exp} = 14.9$; CoNiBpe **2**: $\chi^2 = 2.20$, $R_B = 13.8$, $R_p = 16.4$, $R_{wp} = 21.1$, $R_{exp} = 14.3$; NiCoBpe **3**: $\chi^2 = 2.95$, $R_B = 16.8$, $R_p = 18.4$, $R_{wp} = 24.5$, $R_{exp} = 14.3$; NiBpe **4**: $\chi^2 = 3.56$, $R_B = 7.9$, $R_p = 21.5$, $R_{wp} = 31.5$, $R_{exp} = 16.7$).

The chemical composition was calculated from atomic absorption spectroscopy (AAS) and C, N, H elemental analysis. CoBpe **1** Found: Co 10.3(1), Ni ---; V 17.5(1); C 37.3(2); N 7.3(1); H, 4.4(4); required: Co 10.1, Ni ---; V 17.5; C 37.0; N 7.2; H, 3.6. CoNiBpe **2** Found: Co 5.2(1), Ni 4.9(1); V 17.6(1); C 37.0(1); N 7.2(2); H, 3.6(4); required: Co 5.2, Ni 4.9; V 17.4; C 37.0; N 7.2; H, 3.6. NiCoBpe **3** Found: Co 2.6(2), Ni 7.4(1); V 17.5(2); C 37.2(2); N 7.2(2); H, 3.5(5); required: Co 2.6, Ni 7.4; V 17.5; C 37.0; N 7.2; H, 3.6; NiBpe **4** Found: Co ---, Ni 10.3(1); V 17.6(2); C 37.0(1); N 7.1(3); H, 3.7(4); required: Co ---, Ni 10.1; V 17.5; C 37.0; N 7.2; H, 3.6.

The density was measured by the flotation method in a mixture of bromoform/chloroform being 1.73(3) g cm^{-3} for CoBpe **1**, 1.71(2) g cm^{-3} for CoNiBpe **2**, 1.71(2) g cm^{-3} for NiCoBpe **3** and NiBpe 1.74(2) g cm^{-3} for **4**.

dx.doi.org/10.1021/ic302662x | *Inorg. Chem.* 2013, 52, 2615−2626

Single-Crystal X-ray Diffraction. Single-crystal X-ray diffraction data were collected at 293 K for CoBpe **1** and 100 K for NiBpe **4** on Oxford Diffraction Xcalibur2 (Mo−Kα radiation) and SuperNova Atlas automatic (Cu−Kα radiation) diffractometers, respectively. The Lorentz-polarization and absorption corrections were made with the diffractometer software, taking into account the size and shape of the crystals.[20] The structures were solved by direct methods (SIR-92).[21] The refinement of the crystal structures was performed by full-matrix least-squares based on F^2, using the SHELX97 program.[22] For NiBpe **4** the cell parameters were determined from 30 to 120 °C, each 10 °C.

The crystal structures of **1** and **4** were solved in the $P\bar{1}$ space group, locating all the atoms, except the hydrogen ones. Anisotropic thermal parameters were used for all atoms except the hydrogen ones. The hydrogen atoms belonging to the organic molecule were fixed geometrically, allowed to ride on their parent carbon atoms (C−H = 0.95 Å $U_{Iso}(H) = 1.2U_{eq}(C)$ Å^2), and refined with common isotropic displacements. The hydrogen atoms belonging to the coordinated and crystallization water molecules were located in the Fourier density map and refined with isotropic thermal displacements. For CoBpe **1** compound, the Bpe ligand bonded to the Co(1) cation is disordered in two positions with occupation factors of 0.775(7) and 0.225(7). The disorder was solved assuming equivalence of the chemical equivalent bond lengths and angles, but not torsion angles, of the two disordered Bpe molecules. Equal anisotropic thermal displacements were used for carbon and nitrogen atoms belonging to the disordered Bpe molecules in order to avoid unusual thermal ellipsoids.[23] The inexistence of disorder in the Bpe ligand of the NiBpe **4** crystal structure, determined at 100 K, suggests the existence of the pedal motion mechanism.[24]

Details of crystal, data measuring and reduction, structure solution, and refinement are reported in Table 1. Further details on the crystal structure can be obtained from the CCDC by quoting the depository numbers 909472 for CoBpe **1**, 909473 for NiBpe **4**.

Table 1. Crystal Data and Structure Refinement for CoBpe 1 and NiBpe 4

compound	1	4
formula	$C_{36}H_{42}Co_2N_6O_{18}V_4$	$C_{36}H_{42}N_6Ni_2O_{18}V_4$
fw (g/mol)	1168.38	1167.94
crystal system	triclinic, *P*	triclinic, *P*
color	brown	green
space group, N^{er}	$P\bar{1}$, 2	$P\bar{1}$, 2
a (Å), *b* (Å), *c* (Å)	7.7745 (2), 11.46350(10), 13.5377(2)	7.7086(3), 11.4007(4), 13.4990(3)
A (°), β (°), γ (°)	96.8030(10), 105.710(2), 99.225(2)	96.395(2), 105.619(3), 99.339(3)
Z, *F*(000), *T* (K)	1, 590, 293	1, 592, 100
μ(mm^{-1})	1.59	8.39
crystal size (mm)	0.83 × 0.31 × 0.18	0.31 × 0.24 × 0.14
radiation (λ (Å))	0.71073	1.5418
N^{er} of reflns	7514	4545
reflns ($I > 2\sigma(I)$)	5961	4451
h,*k*,*l* inter	$-11 \geq h \geq 11$, $-17 \geq k \geq 16$, $-19 \geq l \geq 20$	$-9 \geq h \geq 8$, $-14 \geq k \geq 13$, $-12 \geq l \geq 16$
R(int), *R*(sigma)	0.0386, 0.0304	0.024, 0.0288
R_1, wR_2 (obs) ($I > 2\sigma(I)$)	0.0325, 0.082	0.030, 0.0772
R_1, wR_2 (all)	0.0452, 0.0863	0.0299, 0.0775
GOF S	1.02	1.075
N^{er} of parameters/ restraints	317, 18	320, 0
L. diff. peak (e Å^{-3})	1.286	0.098
L. diff. hole (e.Å^{-3})	−0.382	−0.772

Physical Measurements. Infrared spectra were recorded on a Jasco FT/IR-6100 spectrometer with pressed KBr pellets. IR spectra were obtained for the as synthesized samples, and after heating them to 125, 150, 175, 200, 225, and 250 °C, during one hour. Raman spectra were measured on a Ranishaw Raman confocal microscopy spectrophotometer using the 514 nm laser line for excitation. Raman spectra were collected at room temperature, and after heating the samples at 120, 160, and 260 °C until those showed a clear color change. UV−vis diffuse reflectance spectra were registered at room temperature on a Varian Cary 5000 spectrophotometer in the 50000−4000 cm^{-1} range. For CoNiBpe **2**, the study was also carried out after heating the sample at 150, 200, 250, 300, and 340 °C until the sample showed a clear color change. Thermal analyses were performed in air atmosphere, up to 500 °C, with a heating rate of 5 °C min^{-1} on a DSC 2960 Simultaneous DSC-TGA TA Instrument. The temperature dependent PXRD in air atmosphere was realized on a BRUKER D8 ADVANCE Vantec diffractometer (Cu Kα radiation), equipped with a variable-temperature stage (HTK2000) with Pt sample holder. The patterns of CoBpe **1**, CoNiBpe **2**, and NiBpe **4** were recorded each 5 °C from 30 to 400 °C (2θ step = 0.01667°, 2θ range = 5−35°, exposure time = 0.5 s). Magnetic measurements on powdered sample were performed in the temperature range 2−300 K, using a Quantum Design MPMS-7 SQUID magnetometer. The magnetic field was 0.1 T.

Catalytic Study. The cyanosilylation reaction of aldehydes was carried out at 50 °C in the absence of solvent (Scheme 1). CoNiBpe **2** was dried at 100 °C in a vacuum to remove the crystallization water molecules that could interfere with the reaction. Into a screw cap vial with 10 mg of dried CoNiBpe **2**, the aldehyde was added in a rate catalyst/substrate equal to 10:100. The reaction was initiated by the addition of trimethylsilyl cyanide, TMSCN in excess (5 equiv), and the mixture was stirred during the reaction time. The progress of the reaction was monitored by GC-MS analysis. Once the reaction was completed, the solid phase was separated from the liquid by centrifugation. The catalyst was then characterized by powder X-ray diffractometry and IR spectroscopy.

Scheme 1

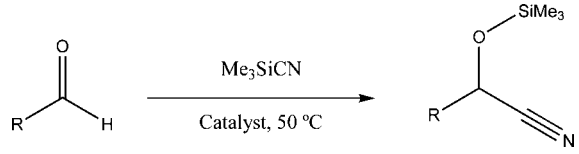

Reuse experiments were carried out for the cyanosilylation of heptaldehyde. The reaction was carried out under the conditions described above. After the reaction completion, the catalyst was recovered by centrifugation, washed with acetone, and dried. The recovered powder was placed in a vial to repeat the reaction in the same conditions twice.

RESULTS AND DISCUSSION

$[\{Co_2(H_2O)_2(Bpe)_2\}(V_4O_{12})]\cdot 4H_2O\cdot Bpe$ **1**, $[\{CoNi(H_2O)_2(Bpe)_2\}(V_4O_{12})]\cdot 4H_2O\cdot Bpe$ **2**, $[\{Co_{0.6}Ni_{1.4}(H_2O)_2(Bpe)_2\}(V_4O_{12})]\cdot 4H_2O\cdot Bpe$ **3**, and $[\{Ni_2(H_2O)_2(Bpe)_2\}(V_4O_{12})]\cdot 4H_2O\cdot Bpe$ **4** are isomorphic. The crystal structures of and **4** have been obtained by single crystal X-ray diffraction. As the compounds are isomorphic, only the crystal structure of the cobalt compound is going to be described, to later establish comparisons of the bond distances and cell parameter evolution of the nickel substituted and nickel compounds.

Crystal Structure. CoBpe **1** crystallizes in the $P\bar{1}$ space group, and its asymmetric unit contains two cobalt atoms laying over inversion centers, two vanadium, six oxygen, one coordinated water molecule, two crystallization water mole-

dx.doi.org/10.1021/ic302662x | Inorg. Chem. 2013, 52, 2615−2626

cules, and three half Bpe molecules. The three-dimensional framework is constructed from inorganic layers pillared by the organic Bpe ligand. The inorganic layers are constructed from corner sharing Co(II) octahedra and (V_4O_{12}) cycles. There are two kinds of Co(II) ions, and both of them are located over inequivalent crystallographic inversion centers. The first octahedra, ($Co(1)N_2O_4$), is bonded to two nitrogen atoms belonging to two Bpe ligands and four oxygen atoms from the (V_4O_{12}) cycle via Co−O−V linkages. The ($Co(2)N_2O_2(H_2O)_2$) octahedron is linked to two Bpe molecules, and two oxygen atoms from two different (V_4O_{12}) cycles. Two coordinated water molecules complete the coordination environment of the Co(2) cation. The bond distances for the cobalt atoms range between 2.1205(16) Å for Co(1)−N(3B) to 2.0572(11) Å for Co(2)−O(4) bonds. The *cis* angles are also near the values for an ideal octahedral coordination environment, with maximum values of 92.34° (O(1)−Co(1)−O(2)) and 91.45° (O(7)−Co(2)−N(1)). The bond distances for the vanadium atoms are in good agreement with the previously reported distances for four coordinated vanadium(V) cations. The shortest bond distance is associated with the V(2)═O(6) terminal bond with a value of 1.6256(11) Å. The maximum V−O bond distance has a value of 1.8067(11) Å. The bond distances of the ($Co(1)N_2O_4$) and $Co(2)N_2O_2(H_2O))_2$ octahedra, and (V_4O_{12}) cycles are depicted in the Table 2.

Table 2. Selected Bond Distances (Å) for CoBpe 1 and NiBpe 4[a]

CoBpe 1		NiBpe 4	
N(3A)—Co(1)	2.1205(16)	N(3)—Ni(1)	2.0966(14)
N(3B)—Co(1)	2.176(8)		
N(1)—Co(2)	2.0982(12)	N(1)—Ni(2)	2.0673(14)
Co(1)—O(1)	2.0651(11)	Ni(1)—O(1)	2.0459(12)
Co(1)—O(2)	2.0849(11)	Ni(1)—O(2)	2.0703(12)
Co(2)—O(4)	2.0572(11)	Ni(2)—O(4)	2.0367(12)
Co(2)—O(7)	2.0750(14)	Ni(2)—O(7)	2.0688(13)
O(2)—V(1)	1.6616(11)	O(2)—V(1)	1.6685(12)
O(3)—V(1)	1.7675(11)	O(3)—V(1)	1.7722(12)
O(5)—V(1)	1.7949(11)	O(5)—V(1)	1.7987(12)
O(4)—V(1)	1.6434(11)	O(4)—V(1)	1.6430(12)
O(3)—V(2)[vi]	1.7924(11)	O(3)—V(2)[vi]	1.7948(12)
O(1)—V(2)	1.6535(11)	O(1)—V(2)	1.6574(12)
O(5)—V(2)	1.8067(11)	O(5)—V(2)	1.8065(12)
O(6)—V(2)	1.6256(11)	O(6)—V(2)	1.6356(12)

[a]Symmetry codes: *x*, −*y*, −*z* + 1; (ii) −*x* + 1, −*y* + 1, −*z* + 1; (iii) −*x*, −*y* + 1, −*z*−1; (iv) −*x* + 1, −*y* + 1, −*z*; (v) −*x*, −*y*, −*z*; (vi) −*x*, −*y* + 1, −*z*.

The (V_4O_{12}) cycles share two oxygen atoms with the ($Co(1)N_2O_4$) octahedra, generating inorganic chains, which are linked through ($Co(2)N_2O_2(H_2O)_2$) octahedra via Co(2)−O(4)−V(1) linkage, generating the inorganic layers shown in the Figure 1.

Bpe organic ligands connect the Co(1) and Co(2) metal centers of adjacent inorganic layers generating the 3D scaffold (Figure 2). The Bpe pillars are slightly tilted generating interlayer channels along the [010] direction, in which one Bpe guest molecule per formula is located. There are several MOFs constructed from carboxylic acids and Bpe ligands exhibiting Bpe guest molecules into the three-dimensional framework.[25] In that regard, several three-dimensional hybrid vanadates with Bpy guest molecules have been also reported, but all of them

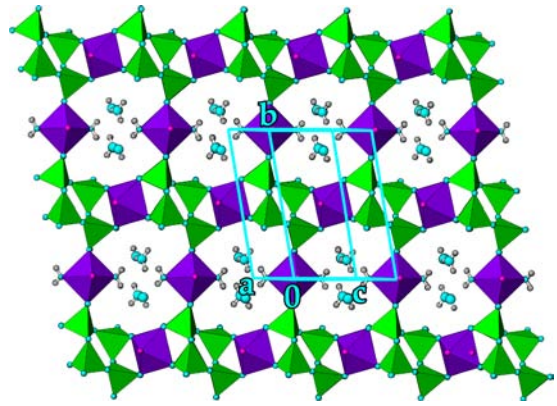

Figure 1. Inorganic layers constructed from CoV_4O_{12} inorganic chains linked through ($Co(2)N_2O_2(H_2O)_2$) octahedral.

are constructed from polioxovanadate cages linked through metal organic nets or chains, instead of the (V_4O_{12}) cycles observed in the title compound.[26] Some examples of polioxovanadates linked via weak interactions to noncoordinated Bpe molecules have been also reported.[27] The $(BpeH_2)_{0.5}[VOF_3]$ hybrid fluorovanadate exhibits ladder like inorganic chains of edge and corner shared VO_5F octahedra. The H_2Bpe ligands and inorganic chains are stabilized by weak interactions.[28] However, based on the search made in the CSD database there are no three-dimensional or two-dimensional hybrid vanadates containing Bpe guest molecules.[29,30]

The polyhedral connectivity in the inorganic layers generates ($Co_4V_6O_{10}$) 20-membered rings. The O(7w) coordinated water molecules belonging to the Co(1) ion point at the center of the ($Co_4V_6O_{10}$) 20-membered rings, establishing four member hydrogen bonds cycle with the O(1w) crystallization water molecules ((O7w)−H(6w)···O(1w) and. O(7w)−H(5w)···O(1w)). The O(2w) crystallization water molecule is connected to the four member hydrogen bonds cycle through the O(1w)−H(2w)···O(2w) hydrogen bond. This crystallization water molecule takes an important role in the stabilization of the Bpe guest molecules in the channels of the crystal structure, through O(2w)−H(4w)···N(2) bonds (Figure 3). The crystallization water molecules also establish hydrogen bonds with the oxygen atoms belonging to the VO_4 tetrahedra of the inorganic layers (O(2w)−H(3w)···O(6) and O(1w)−H(1w)···O(2)). Table S1 includes the hydrogen bonding information for CoBpe **1** and NiBpe **4** compounds.[31]

The crystal structure can also be described as a simplified net.[32] The simplification was carried out considering the (V_4O_{12}) cycles, ($Co(2)N_2O_2(H_2O)_2$), and ($Co(2)N_2O_4$) octahedra as nodes and the Bpe organic ligands as linkers of the net. The topological analysis gives rise to a three nodal four-connected 4,4,4T47 (TotUMod) net with $\{6^4.8^2\}_2\{6^6\}$ point symbol. As far as we are concerned this is the first compound exhibiting this topological type. Moreover, the crossed disposition of the Bpe pillars between the inorganic layers generates a self-catenated net.

The evolution of the cell parameters with respect to the Co(II) percentage of the compounds is shown in the Figure S1. In good agreement with Vegard's Law, the cell volume and parameters increase progressively with the introduction of Co(II) (0.745 Å) instead of Ni(II) (0.690 Å), because of the difference between the ionic radii of the octahedrically coordinated high spin Co(II) ions and Ni(II) cations. The introduction of cobalt in the crystal structure generates an

dx.doi.org/10.1021/ic302662x | *Inorg. Chem.* 2013, 52, 2615−2626

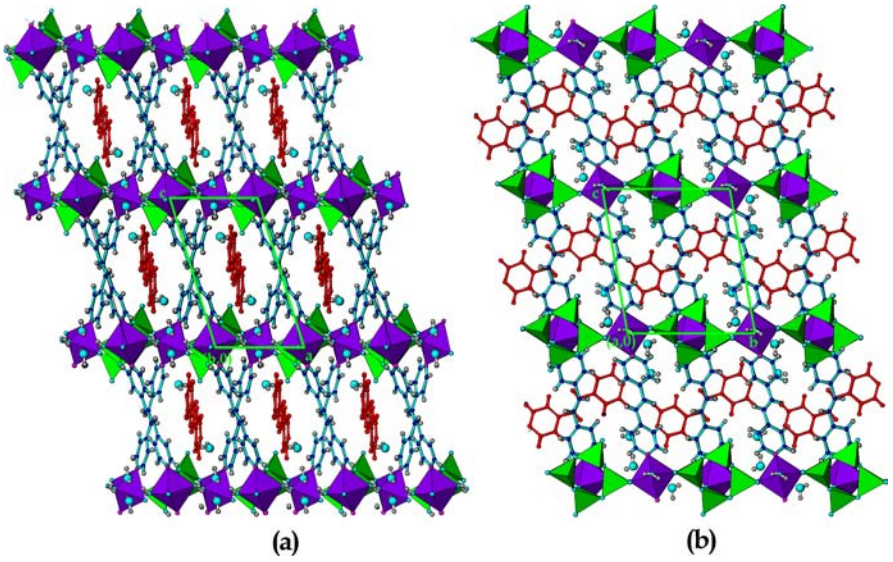

Figure 2. Crystal structure of the 3D inorganic scaffold with Bpe organic ligand located at the [010] channels of the inorganic−organic scaffold. (a) [010] view. (b) [100] projection.

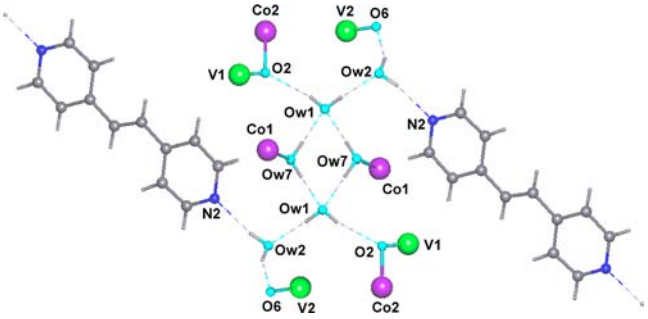

Figure 3. Hydrogen bonding between the coordinated water molecules (O(w7)), crystallization water molecules (O(w1), O(w2)), and the Bpe guest molecules.

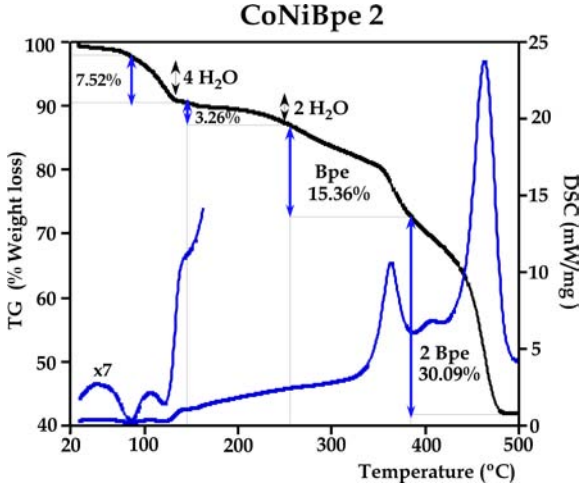

Figure 4. TG and DSC curve for the CoNiBpe **2** compound.

increase of the interlayer distance related to "c" parameter and a slight expansion of the inorganic layers related to the increase of "a" and "b" parameters.

Physic-Chemical Properties. *Thermal Stability.* The TGA and DSC curves resulting from the thermogravimetric analysis of **1**−**4** are shown in the Figure 4 and Figure S2. The weight losses and temperature ranges for the four decomposition steps of the compounds are depicted in Table S2.

The thermal decomposition of the studied compounds is initiated by the loss of four crystallization water molecules in the 80−140 °C temperature range (calc. 6.14%). The DSC curve shows two exothermic peaks suggesting a two-step water molecules release, in good agreement with the existence of two crystallographic independent crystallization water molecules. The second and the third decomposition steps are partially overlapped and correspond to the removal of the coordinated water molecules (calc. 3.07%) and guest Bpe molecule (calc. 15.52%). Finally, the structural collapse takes place with the calcination of the two Bpe molecules per formula that act as pillars between the inorganic layers (calc. 31.04%). The TG curves are very similar for all the studied compounds, but the loss of coordinated water molecules and Bpe guest molecules begins at higher temperatures for the compounds containing nickel.

The thermal behaviors of **1**, **2**, and **4** were studied also by thermodiffractometry. The thermal evolution of (001) and (010) reflections is shown in Figure 5. Two main transformations related to the loss of the crystallization water molecules and coordinated water molecules are observed. The release of the crystallization water molecules takes place in a short-range of temperatures (110−120 °C). This process gives rise to a drastic reduction of the crystallinity and displacements of (001) and (010) reflection to higher 2θ values. This behavior is in good agreement with the previously reported thermal behaviors for hybrid vanadates containing coordinated water molecules.[33] The crystallinity decrease is clearly related with the importance of the hydrogen bonding network established between the crystallization, coordinated water molecules and Bpe guest molecules. The crystal framework becomes more disordered after the release of the crystallization water molecules. The displacements of the (001) and (010) reflections to higher 2θ values imply a reduction of the interlayer distance and also a contraction of the inorganic layers along the [010] direction. The loss of coordinated water molecules occurs in a wide range of temperatures (200−280

dx.doi.org/10.1021/ic302662x | *Inorg. Chem.* 2013, 52, 2615−2626

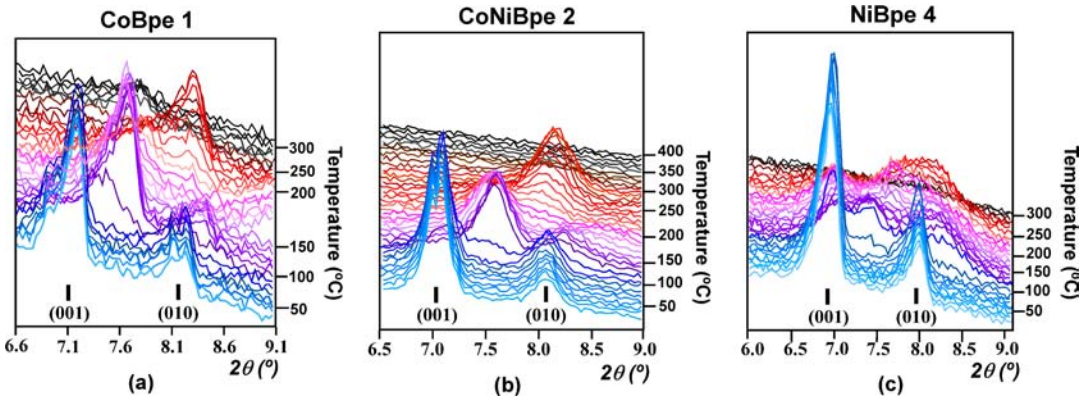

Figure 5. (a–c)Thermal evolution of the (001) and (010) peaks for the **1**, **2**, and **4** compounds.

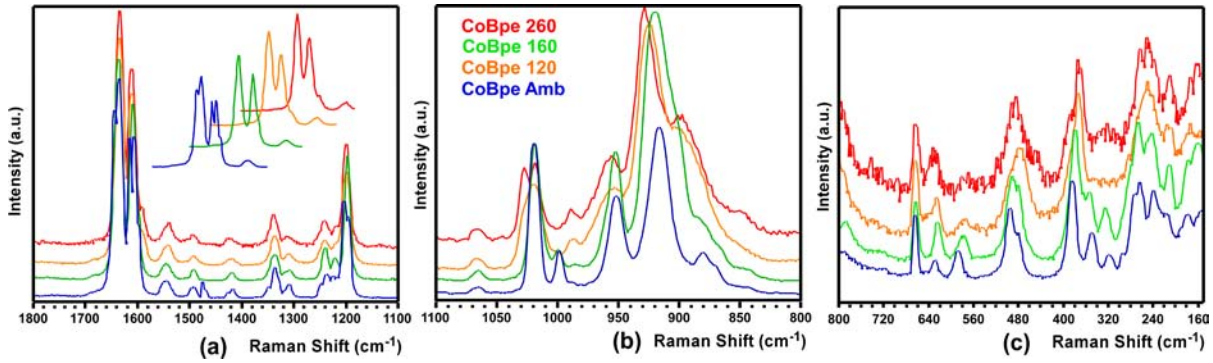

Figure 6. Raman shift (cm^{-1}) for CoBpe **1**, and after heating the compound at 120, 160, and 260 °C. (a) Bpe ligand vibrational interval, (b) (V_4O_{12}) cycles adsorption, (c) the low value Raman shift associated to the M–O, M–py, and M–H_2O bonds.

°C). During the process, the patterns show a drastic reduction of the crystallinity, and only the (001) maximum is observed after the transformation. The displacement of the (001) maximum to a higher 2θ values indicates a second contraction of the "c" parameter, and hence, a shortening of the interlayer distance. Despite the crystallinity reduction, the presence of the (001) reflection in the patterns confirms that the layered structure is maintained after the release of crystallization and coordinated water molecules, at least in the CoBpe **1** and CoNiBpe **2** compounds.

With regard to NiBpe **4**, the crystal structure behaves different during the transformations. At temperatures upon 110 °C there is also a crystallinity reduction, and three very broad maxima replace progressively the (001) and (010) peaks of the initial phase. The thermal evolution of the cell parameters for NiBpe **4** has been obtained by single crystal X-ray diffraction (Figure S3). After the loss of crystallization water molecules, the diffraction spots become more elongated and diffuse, in good agreement with the loss of crystallinity observed by powder X-ray diffraction. At temperatures above 140 °C the crystallinity is too low to determine the cell parameters. The first transformation takes place between 110 and 120 °C and involves a reduction of 7% (80 $Å^3$) of the cell volume. The thermal evolution of the cell parameters allows a qualitative description of the structural changes. Thus, the loss of crystallization water molecules gives rise to a tilting of the Bpe organic pillars between the inorganic layers and hence an increase of the "α" angle value. Moreover a 4% reduction of the "c" parameter, related with the decrease of the interlayer distance, is also observed. The layered structure is stable up to 140 °C but at higher temperatures is difficult to determine any qualitative structural information from X-ray diffraction. Above 140 °C, there are slight and progressive changes in the intensity and position of these three main broad maxima due to the progressive removal of coordinated water molecules.

Spectroscopic Properties. *Infrared and Raman Spectroscopies.* The IR and Raman spectra of the as-synthesized **1**–**4** compounds are very similar. Three main regions can be distinguished: (i) the absorption maxima related with the crystallization and coordinated water molecules (3700–3000 cm^{-1}), (ii) the Bpe ligand vibrational modes generating absorption maxima in the 1700 to 1000 cm^{-1} range, and (iii) the absorption bands located at frequencies below 1000 cm^{-1}, associated with (V_4O_{12}) cycles, and tentatively assigned to the V=O streching (1000–900 cm^{-1}), $V_{as}(VO_4)^{-3}$ (890 (s) cm^{-1}), and V_{as}(V–O–M) 725(s) vibrations. In the Raman spectra, the low Raman shift interval (600–140 cm^{-1}) contains also the vibrational information about the M–O, M–py, and M–H_2O bonds, M=Ni, Co.[34] Furthermore, the IR and Raman spectra were also recorded after heating the samples at different temperatures during one hour. The evolution for the more representative absorption bands are depicted in Figures 6, S4 and S5. The most representative experimental vibration frequencies (cm^{-1}) and assignment of vibrational modes are shown in Table S3.

Three main signals for the stretching vibration of the O–H bonds are observed in the IR spectra at 3500, 3450, and 3175 cm^{-1} (Figure S4a). The outcome of the crystallization (125 °C) and coordinated water molecules (>175 °C) gives rises to the decrease of the absorbance for the bands located in the 3600–3000 cm^{-1} range. (Figure S4 (a.1–a.3)). With regard to the organic ligand, the position and intensity of the related bands,

dx.doi.org/10.1021/ic302662x | Inorg. Chem. 2013, 52, 2615–2626

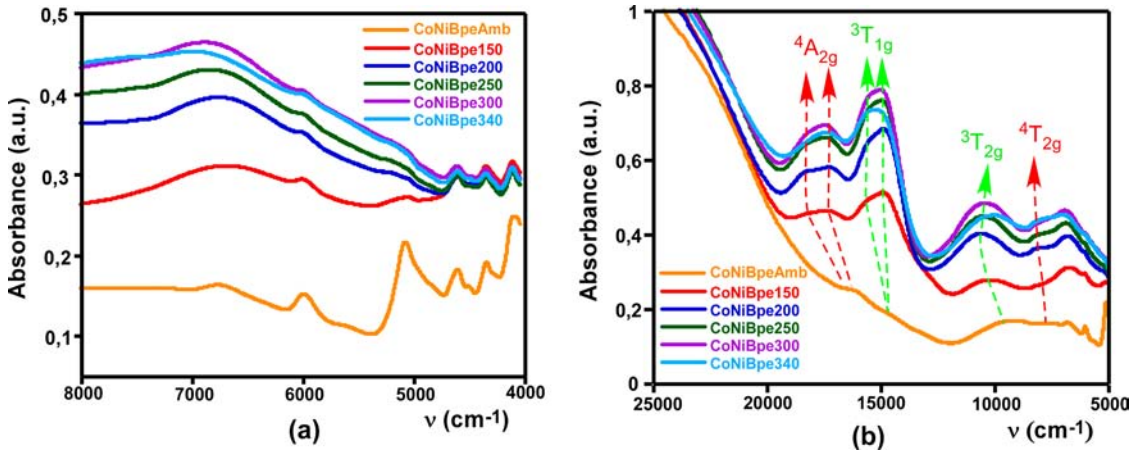

Figure 7. UV−vis spectra for the CoNiBpe **2** compound after thermal treatments at 150, 200, 250, 300, and 340 °C. (a) 8000−4000 cm^{-1} interval associated to the absorption of the Bpe organic ligand and water molecules. (b) 25000−5000 cm^{-1} range showing the absorption maxima related with the Co(II) and Ni(II) cations.

such as ν(C═C) or δ(ring), change slightly in the heated samples (Figure S4 (b.1−b.3)), confirming that the structural transformations affect more the position and orientation of the Bpe pillars and Bpe guest molecules than the ligand coordination or the ligand itself. This fact is in good agreement with the tilting of the Bpe pillars and the interlayer distance shortening after the loss of crystallization water molecules, observed by X-ray diffraction studies.

The main changes in the IR spectra are observed in the vanadate oxoanion absorption range (Figure S4 (c.1−c.3)). The IR-spectra (at 150 °C) of the CoBpe **1** and NiBpe **4** compounds become different after losing the crystallization water molecules. For the cobalt compound the intensity of the bands strongly changes, while for the nickel compound remain almost equal. The IR spectroscopy confirms that the crystal structures of the nickel and cobalt compounds possess different responses to the release of crystallization water molecules. CoNiBpe **2** shows a behavior close to the CoBpe **1** compound. Despite the intensity changes, after the loss of crystallization water molecules the absorption bands remain approximately at the same position. This fact suggests that the structural building blocks (V_4O_{12}) cycles, metal octahedra, and Bpe ligands are slightly reorganized to balance the outcome of the crystallization water molecules. After the removal of coordinated water molecules, above 175 °C, the absorption bands related to the vanadate oxoanion change progressively up to 250 °C. Again, the spectra observed at 250 °C for the NiBpe **4** and CoBpe **1** compounds are different, but the absorption maxima related to the vanadate group are still observed.

Raman spectra do not show differences in the transformation processes between cobalt and nickel compounds. The most representative absorption ranges are shown in Figure 6 for CoBpe **1**. The spectra for CoNiBpe **2** and NiBpe **4** are depicted in Figure S4. The as-synthesized CoBpe **1** compound shows two different strong bands related to the $\nu(C{=}C)_v$ vibrational mode and other two associated to the pyridil ring $\nu(C{-}N)_p$, $\nu(C{-}C)_p$ and $\delta(C{-}H)_p$ vibrations. These two signals are related to the Bpe ligands joined to the metal centers and the Bpe organic molecule located into the channels of the crystal structure, respectively. The bands are shifted to the same position after the crystallization water molecules (120 °C) are removed.

The absorption bands related to the (V_4O_{12}) cycle are located between 1100 and 800 cm^{-1} absorption range. There is a clear intensity change between the room temperature spectra and the one recorded after heating the sample at 120 °C, but no drastic changes in the bands positions are observed.

The most important change is related to the band located at 1000 cm^{-1} in the room temperature spectrum, which loses intensity and shifts to lower frequencies at higher temperatures. This band is related to the υ(V═O) stretching vibration, suggesting that the V═O terminal bonds of the (V_4O_{12}) cycles disappear after the loss of coordinated water molecules.[35]

At low Raman shift values (Figure 6c), the absorption band located at 320 cm^{-1}, tentatively assigned to the M−H_2O stretching vibration, disappears when the samples are heated up to 160 °C, indicating the loss of the coordinated water molecules. The bands related to the (V_4O_{12}), M−O, M−N, and M−py vibrational modes change their position slightly for the samples heated at 120, 160, and 260 °C. As a general trend of the Raman spectra, a progressive widening of the absorption maxima is observed when the samples are heated. This fact is in good agreement with the loss of crystallinity, and hence less ordered crystal structures, after the transformations of the compounds.

The UV−vis spectra for **1**−**4** are depicted in Figure S6. The CoBpe **1** and NiBpe **4** absorption spectra contain the characteristic absorption bands for octahedrically coordinated high spin Co(II) d^7 and Ni(II) d^8 cations. For **1** the broad band located at 7500 cm^{-1} and the shoulder at 16125 cm^{-1} are assigned to the $^4T_{1g} \rightarrow {}^4T_{2g}$ and $^4T_{1g} \rightarrow {}^4A_{2g}$ spin allowed transitions, respectively; while for **4** the absorption bands at 9450 and 15400 cm^{-1} are attributed to the $^3A_{2g} \rightarrow {}^3T_{2g}$ and $^3A_{2g} \rightarrow {}^3T_{1g}$ allowed transitions. From the spin transitions corresponding to the d^8 and d^7 high spin Co(II) d^7 and Ni(II) d^8 cations in octahedral geometry, the D_q and Racah B parameter have been calculated, using the energy expressions given in the Tanabe-Sugano diagrams (CoBpe **1**: D_q = 863 cm^{-1}, B = 680 cm^{-1}; NiBpe **4**: D_q = 945 cm^{-1}, B = 880 cm^{-1}). The values of the Racah parameters B are approximately the 61% and 85% of the free Co(II) and Ni(II) cations, respectively, revealing an appreciable covalent character in the M−O, M−H_2O, and M−N chemical bonds. As is expected, the CoNiBpe **2** and NiCoBpe **3** compounds possess intermediate spectra between the nickel and cobalt phases.[36]

dx.doi.org/10.1021/ic302662x | Inorg. Chem. 2013, 52, 2615−2626

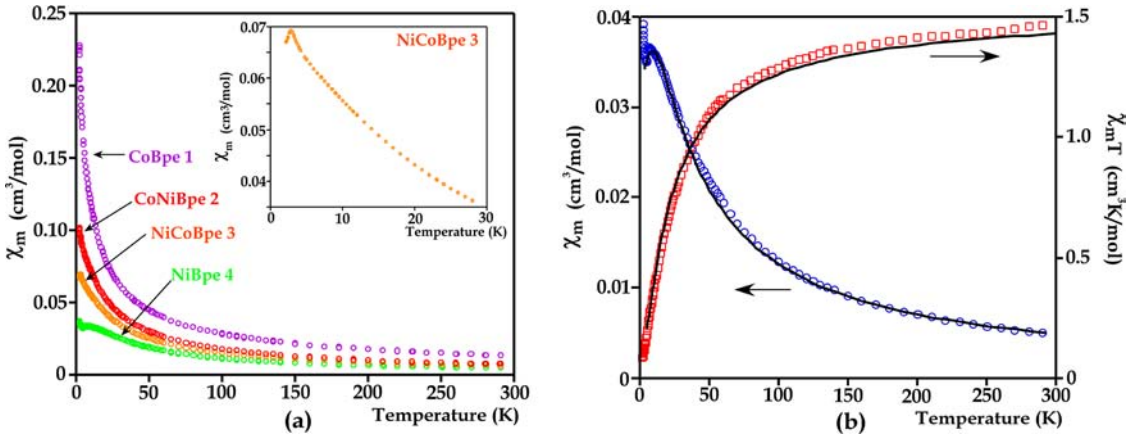

Figure 8. (a) Thermal evolution of χ_m curves for **1**–**4** compounds. (b) Fitting of the χm and $\chi_m T$ curves with a isotropic chain S = 1 model for NiBpe **4**.

The high reaction yield achieved in the synthesis of CoNiBpe **2** compound has allowed obtaining enough quantity of material to carry out the study of thermal evolution of UV–vis spectroscopy after heating the sample to 150, 200, 250, 300, and 340 °C. The results are shown in Figure 7. The 8000 to 4000 cm^{-1} spectral region focuses the absorption bands related to the organic Bpe ligand and water molecules (Figure 7a).

The absorption interval containing the allowed transitions for the Ni(II) and Co(II) cations (25000–5000 cm^{-1}) is shown in Figure 7b. The maximum located at 5000 is related to the crystallization and coordinated water molecules and practically disappears after heating the sample up to 150 °C. The shoulder observed in the spectra recorded after heating the samples to 200, 250, 300, and 340 °C is generated by the water molecules adsorbed during the sample transfer from the furnace to the spectrometer. The crystallization and coordinated water molecules cannot be distinguished in the UV–vis spectra. After the removal of water molecules (150–250 °C) the spin transitions Co(II) $^4T_{1g} \rightarrow {}^4A_{2g}$ and Ni(II) $^3A_{2g} \rightarrow {}^3T_{1g}$ split in two different positions (Figure 7b), shifting to higher frequency values. The absorbance of the bands related to Co(II) and Ni(II) cations also increases at temperatures higher than 150 °C. Taking into account the position of the absorption bands the coordination environment of the Ni(II) and Co(II) cations is still octahedral after the removal of crystallization (150 °C) and coordinated water molecules (250 °C). The splitting and absorbance increase of the bands imply a distortion of the octahedral coordination environment of the metal centers after the structural transformations. As is expected by the thermogravimetric curve, the Bpe guest molecules release begins at temperatures higher than 280 °C. No variation in the intensity of the bands related to the Bpe molecule is observed at 300 and 340 °C, but the intensity of the absorption maxima associated with the metal centers slightly decreases. Co(II) and Ni(II) cations are still octahedrially coordinated when Bpe guest molecule loss begins.

Pictures were taken after the removal and uptake of crystallization and coordinated water molecules in order to characterize the color changes (Figure S7). As it has been observed in the IR spectroscopic study, NiBpe **4** exhibits a different color change in comparison with the CoNiBpe **2** and CoBpe **1** compounds. For NiBpe **4**, the color changes from a pale green to a pale yellow during the heating process. The initial color is only recovered for the sample heated at 100 °C. CoBpe **1** and CoNiBpe **2** compounds possess pale orange colors. At temperatures higher than 150 °C the color changes to green, becoming darker when increasing the temperature. This fact is in good agreement with the shifting and increase of absorbance for the absorption bands observed in the UV–vis. The process is reversible up to temperatures as high as 275 °C, but the initial color is slightly darkened when the sample is thermally treated, so, probably, a small percentage of sample does not recover the hydrated initial stage. An interesting point is that the samples heated up to 200 °C recover the crystallization and coordinated water molecules in a few seconds, only exposing them to ambient conditions. The uptake of water for the samples heated at 250 and 275 °C is slower, and the initial color is not completely recovered.

The powder X-ray diffraction study shows that compounds containing cobalt (**1**–**3**) show a complete and reversible removal/uptake of crystallization and coordinated water molecules (Figure S8). For CoNiBpe **2** the removal/uptake of water molecules was studied by thermodiffractometry revealing that the process is completely reversible up to 290 °C, the temperature at which the compound becomes amorphous (Figure S9). For NiBpe **4**, after heating the sample up to 275 °C and rehydrating at room temperature, the pattern shows clear differences with the pattern of the as-synthesized sample.

Magnetic Properties. Magnetic measurements were performed on powdered samples from room temperature to 2 K, at a magnetic field of 0.1 T. The thermal evolution of the molar susceptibility χ_m and χ_m vs T are shown in Figure 8.

For CoBpe **1** and CoNiBpe **2** compounds, the molar susceptibility χ_m curves show a continuous increase on cooling to maximum values of 0.228 cm^3/mol for **1** and 0.102 cm^3/mol for **2** (inset Figure 8a). For NiCoBpe **3** a sharp maximum at 3 K (0.069 cm^3/mol) is observed. Below this temperature the magnetic susceptibility decreases down to (0.067 cm^3/mol) (inset Figure 8). The thermal dependence of χ_m for NiBpe **4** shows a broad maximum at 7 K (0.034 cm^3/mol) and a sharp increase of the χ_m value below 4.5 K to a maximum value of 0.037 cm^3/mol at 2K (Figure 8b).

The inverse susceptibilities are well fitted below 100 K for **1** and 50 K for **2**, **3**, and **4** to a Curie–Weiss law. The C_m and θ calculated values are depicted in Table 3. The Curie constant value for NiBpe **4** (1.62 cm^3 K/mol) is greater than the expected for an isolated Ni(II) cation (S = 1, g = 2.2, C_m = 1.21

dx.doi.org/10.1021/ic302662x | Inorg. Chem. 2013, 52, 2615–2626

Table 3. Main Magnetic Data for Compounds 1−4

compound	T^{re} range	C_m (cm^3 K/mol)	θ (K)
CoBpe **1**	300−100	3.31	−32
CoNiBpe **2**	300−50	2.33	−36
NiCoBpe **3**	300−50	2.09	−27
CoBpe **4**	300−50	1.62	−37

cm^3 K/mol) due to the contribution of the temperature-independent paramagnetism typical for the Ni(II) ion. The experimental value for CoBpe **1** is inside the values observed for a high spin Co(II), $S = 3/2$ cation (2.3−3.5 cm^3 K/mol). The negative Weiss temperatures for all the studied compounds reveal an antiferromagnetic coupling between the metal centers at high temperatures.[37]

Due to the large distance between the M(II) ions connected by the Bpe ligand (M(1)−M(1): 13.66 Å and M(2)−M(2): 13.54 Å) significant exchange interactions through this magnetic exchange pathway are not expected. The shorter distances between the metal ions are located within the inorganic layers. The M(1)···M(2) distance connected through on VO_4 tetrahedron is 6.39 Å, and the connectivity between the metal centers across the O−V−O atoms suggests the existence of a main one-dimensional magnetic pathway J_1. The magnetic exchange pathway J_2 between adjacent chains involves a M(1)···M(1) distance of 7.77 Å, and the metal centers are connected through two VO_4 tetraedra (M−O−V−O−V−O−M), so the magnetic interaction is expected to be very weak. Taking into account the possible magnetic exchange pathways, for NiBpe **4** compound, the thermal evolution of the molar susceptibility χ_m was fitted in the 300 to 12 K temperature range to an isotropic one-dimensional chain magnetic model for Ni(II) $S = 1$ cation (eq 1).

$$Xm = \frac{N}{3kT}\frac{\beta^2 g_1{}^2 S(S+1)(1+u_1)}{(1-u_1)} + \mathrm{TIP};\ u = \left(\coth\frac{JiS(S+1)}{kT}\right) - \left(\frac{kTS(S+1)}{Ji}\right) \quad (1)$$

In eq 1, N is Avogadro's number; β, Bohr magneton; g, gyromagnetic ratio; k, Boltzmann's constant; T, absolute temperature; and the term TIP takes into account the temperature independent paramagnetism.

The best fitting parameters obtained are $g = 1.960(2)$, $J/k = -11.65(2)$ K and TIP = 0.0025(2) cm^3/mol. The J/k negative value indicates the one-dimensional antiferromagnetic coupling between Ni(1) and Ni(2) cations.

For NiCoBpe **3** and NiBpe **4** and compounds molar susceptibility maxima are observed below 7 and 3 K. These maxima could be related with a 2D antiferromagnetic ordering of the adjacent one-dimensional chains within the inorganic layers through the J_2 magnetic exchange pathway. The anisotropy of the cobalt cation favors the one-dimensional antiferromagnetic coupling at low temperatures, and hence, no maxima observed in the magnetic susceptibilities of CoBpe **1** and CoNiBpe **2**.

Catalytic Study. Cyanosilylation reactions are important C−C bond forming reactions catalyzed by Lewis acids.[38] CoNiBpe **2** was proved as catalyst in the cyanosilylation reaction of aldehydes with TMSCN under solvent-free conditions. The reaction conditions were first established using benzaldehyde as model substrate. The best conversion rates were obtained when using 10% of catalyst at 50 °C. Once the conditions were established, different aldehydes were used to study the scope of the reaction. Results were summarized in Table 4. When using aromatic aldehydes, the conversion

Table 4. Conversion Rates (%) of Cyanosilylation Reactions for CoNiBpe 2

substrate	time (h)	C_T (%)
benzaldehyde	16	77
p-methylbenzaldehyde	16	82
p-fluorobenzaldehyde	16	37
heptaldehyde	6	97

decreases in the order *p*-methylbenzaldehyde > benzaldehyde > *p*-fluorobenzaldehyde, in agreement with their corresponding electronic effects. When using an aliphatic aldehyde as heptaldehyde, the reaction takes place faster than when using aromatic aldehydes.

After the reactions, the solid catalyst was recovered by centrifugation and washed with dichloromethane and acetone and then characterized by powder X-ray diffraction and IR spectroscopy. The powder diffraction patterns of the recovered catalysts are very similar to the as synthesized CoNiBpe **2** pattern. However, a widening of the diffraction maxima is observed (Figure S10). On the other hand, the IR spectra show two extra bands with regard to the as-synthesized compound. These two bands appeared at 2135 and 2165 cm^{-1} and are due to the existence of cyanide groups (Figure S11). This fact suggests that the excess of TMSCN is bonding to the metallic centers through the nitrogen atom. This may reduce the activity of the catalyst for its reuse, as can be observed later in the recycling test.

Reutilization is one of the greatest advantages of heterogeneous catalysts and can also provide useful information about the anchoring process and catalyst stability along the catalytic cycle. Recycling tests were carried out over CoNiBpe **2** for the cyanosilylation of heptaldehyde. The catalyst was recycled three runs. During the successive cycles, a decrease in the activity was observed (Figure 9).

The recovered catalyst was washed with dichloromethane and acetone and characterized by X-ray powder diffraction and IR spectroscopy. After three runs the only diffraction maximum in the X-ray pattern corresponds to the (001) plane (Figure S10). The position of the maxima is approximately the same

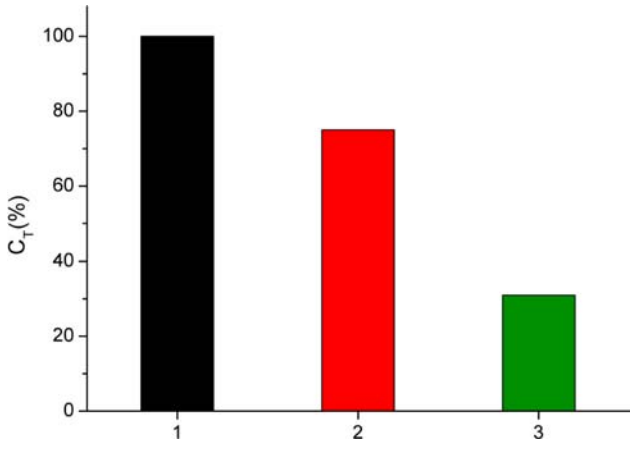

Figure 9. Recyclability of compound **2**.

dx.doi.org/10.1021/ic302662x | *Inorg. Chem.* 2013, 52, 2615−2626

that in the as-synthesized compound. This fact confirms that the layered structure and interlayer spacing are maintained after the catalysis reactions, but the crystallinity loss indicates that CoNiBpe **2** is progressively degraded. On the other hand, the IR spectrum shows the above-mentioned extra bands at 2135 and 2165 cm^{-1} due to the existence of cyanide groups (Figure S11). Therefore, the activity decrease can be explained by the successive blocking of the active centers by cyanide groups along the consecutive cycles. It seems quite plausible that the reaction goes via displacement of the labile Co/Ni−OH_2 bond by aldehyde before its activation and reaction (Figure S12). However, we do not have evidence to affirm that the reaction takes place via this proposed mechanism. The active center blocking, on the other hand, is not related with the reaction mechanism, but with the excess of TMSCN in the reaction media. The IR spectra of the catalyst after the reaction show that there are cyanide groups. According to the literature, C≡N stretching band of free TMSCN is observed at 2191 cm^{-1}. The shift of this band to higher ν values indicates that the adsorption of TMSCN onto the surface of CoNiBpe **2** occurred through the C≡N π system.[39] Further studies are going to be carried out in future works to corroborate this hypothesis.

CONCLUSIONS

There are few examples of metal organic frameworks constructed from inorganic layers pillared by organic ligands that contain large molecules, as Bpe, in the framework's channels. The crystal structures of **1**−**4** reveal the importance of the hydrogen bonding network between the coordinated water molecules and guest molecules (crystallization water and Bpe guest molecules) in the thermal stability of the crystal framework. In fact, the release of crystallization water molecules break the hydrogen bonding network of the initial crystal structure, giving rise to a loss of the short-range order. This is well understood taking into account the great degree of freedom and motion that possess the Bpe guest molecules to readjust their position after the removal of crystallization water molecules. In fact, a clear reduction of the interlayer distance is observed in the shift of the (001) reflection to higher 2θ values. In contrast to the removal of crystallization water molecules, with a very sharp response of the crystal structure in a short-range of temperature (100−120 °C), the departure of the coordination water molecules takes place progressively and probably could be partially overlapped with the beginning of the Bpe guest molecules loss. The crystal structure also responds to the removal of coordinated water molecules with a second reduction of the interlayer distance. Despite the drastic reduction of crystallinity after the transformations, the IR, Raman, and UV−vis experiments prove that the initial building blocks of the crystal structure still remain approximately unchanged after the release of crystallization and coordination water molecules. The coordination environment of the metal centers is still octahedral after the loss of the coordination water molecules, suggesting that new metal−oxygen bonds are generated, probably involving the V(2)═O(6) terminal bonds belonging to the (V_4O_{12}) cycles. This hypothesis is supported by the disappearance of the Raman shift bands related to the M−H_2O and V═O bonds, when the samples are heated up to 150 °C.

The loss of the coordinated water molecules (>150 °C) involves a clear color change of the samples, so the coordination environment of the Co(II) and Ni(II) metal centers are distorted in this structural transformation. Moreover, the coordinated water molecules can be uptaken in the crystal structure reversibly just in a few seconds, by exposing the samples to ambient conditions. However, the thermal treatments up to 250 °C hinder the complete recovering of the initial color. The mechanism of transformation is poorly understood. The IR and Raman studies prove that the initial building blocks remain approximately unchanged, but it is not clear how the coordination environment of the metal centers is completed after the removal of coordinated water molecules. The rational design of the crystal structures, and more specifically, the rational choice of initial structural building blocks with enough degree of freedom to establish new weak interactions and/or bonds is a essential task to avoid the crystalline to pseudoamorphous transformations after the loss of coordinated species. In that regard, different possible strategies can be adopted, such as (i) the synthesis of crystal structures containing not rigid inorganic substructures formed by corner-sharing polyhedra, (ii) the choice of secondary metal centers that could adopt different coordination environments, such as Co(II) and Cu(II); and (iii) the use of flexible organic ligands, instead of Bpe, that not only could reorient themselves or adopt different conformations, but may also incorporate not bridging atoms to the coordination sphere of the secondary metal centers.

The magnetic behaviors of the compounds are also affected by the molar Co/Ni relation in the crystal structures. All the compounds show an antiferromagnetic one-dimensional coupling of the metal centers, but NiCoBpe **3** and NiBpe **4** phases also exhibit an antiferromagnetic ordering at low temperatures. This order is not observed for the CoBpe **1** and CoNiBpe **2** compounds, probably because the magnetic anisotropic character of Co(II) favors the one-dimensional coupling observed at high temperatures. As was proved with CoNiBpe **2**, this family of materials can act as heterogeneous catalysts in the cyansilylation reactions of aldehydes. However, the excess of TMSCN used in this reaction blocks the active centers of the catalysts, making them less active for their reutilization.

ASSOCIATED CONTENT

Supporting Information

Figure S1: Cell parameters (Å), angles (°), and volume ($Å^3$) evolution in function of the Ni/Co content in **1**−**4** compounds. Figure S2: TG and DSC curve for the studied **1**−**4** compounds. Figure S3: Thermal evolution of the cell parameters in the 30−140 °C temperature range for NiBpe **4**. Figure S4: Selected IR spectra intervals (a) water molecules absorption, (b) Bpe organic ligand absorption, and (c) (V_4O_{12}) cycles adsorption. Figure S5: Raman spectra for the CoNiBpe **2** and NiBpe **4** as-synthesized compounds, and after heating those to 120, 160, and 260 °C. Figure S6: UV−vis spectra for **1**−**4** compounds. Figure S7: Pictures of NiBpe **4**, CoNiBpe **2**, and CoBpe **1** samples after thermal treatments at different temperatures. Study of the recovering of the initial color after the heating process. Figure S8: X-ray diffraction patterns of the samples after a thermal treatment at 275 °C. Blue pattern: CoNiBpe **2** as-synthesized sample. Figure S9: Thermal treatment for the CoNiBpe **2** sample. The patterns are recorded at 130, 220, and 290 °C, and after lowering the temperature to 30 °C. Figure S10: X-ray diffraction patterns of as-synthesized CoNiBpe **2** compound and recycled CoNiBpe **2** after the cyanosilylation reactions. Figure S11: IR spectra of as-synthesized CoNiBpe **2** compound and recycled CoNiBpe **2** after the cyanosilylation

dx.doi.org/10.1021/ic302662x | Inorg. Chem. 2013, 52, 2615−2626

reactions. Figure S12: Proposed reaction mechanism via displacement of the labile Co/Ni−OH^2 bond by aldehyde before its activation and reaction. Table S1: Hydrogen bonding (Å) and angles (°) for CoBpe **1** and NiBpe **4**. Table S2: Weight loss observed in the different decomposition stages of the TG curves for **1**−**4** compounds. Table S3: Raman and IR absorption bands and assignment of the different vibrational modes for the water molecules, Bpe organic ligand, C_i symmetry (V_4O_{12}) cycles and M−O, M−H_2O, and M−N bonds. Crystallographic information files (CIF). This information is available free of charge via Internet at http://pubs.acs.org/.

AUTHOR INFORMATION

Corresponding Author

*E-mail: maribel.arriortua@ehu.es. Phone: 34-946012534. Fax: 34-946013500.

Notes

The authors declare no competing financial interest.

ACKNOWLEDGMENTS

This work has been financially supported by the "Ministerio de Ciencia e Innovación" (MAT2010-15375 and MAT2011-29020-C02-02) and the "Gobierno Vasco" (IT-177-07), which we gratefully acknowledge. The authors thank the technicians of SGIker (UPV/EHU), Drs. J. Sangüesa, A. Larrañaga, P. Vitoria, and I. Orue, financed by the National Program for the Promotion of Human Resources within the National Plan of Scientific Research, Development and Innovation, "Ministerio de Ciencia y Tecnología" and "Fondo Social Europeo" (FSE), for the X-ray diffraction and magnetic measurements, respectively. R. Fernández de Luis thanks to the MICINN (Madrid, Spain) (BES-2005-10322). E. S. Larrea thanks the UPV/EHU for funding.

REFERENCES

(1) Kickelbick, G. *Hybrid Materials. Synthesis, Characterization, and Applications*; Wiley-VCH: Weinheim, Germany, 2007; Chapter 1, pp 1−48.

(2) (a) Savonnet, M.; Canivet, J.; Gambarelli, S.; Dubois, L.; Bazer-Bachi, D.; Lecocp, V.; Bats, N.; Farrusseng, D. *CrystEngComm* **2012**, *14*, 4105−4108. (b) Ahigematsu, A.; Yamada, T.; Kitagawa, H. *J. Am. Chem. Soc.* **2012**, *134*, 13145−13147. (c) Sadakiyo, M.; Okawa, H.; Shigematsu, A.; Ohba, M.; Yamada, T.; Kitagawa, H. *J. Am. Chem. Soc.* **2012**, *134*, 5472−5475.

(3) (a) Férey, G. *Chem. Soc. Rev.* **2008**, *37*, 191−214. (b) Kitagawa, S.; Kitaura, R.; Noro, S.-I. *Angew. Chem., Int. Ed.* **2004**, *43*, 2334−2375. (c) Calderón-Casado, A.; Barandika, G.; Bazán, B.; Urtiaga, M.-K.; Vallcorba, O.; Rius, J.; Miravittles, C.; Arriortua, M. I. *CrystEngComm* **2011**, *13*, 6831−6838.

(4) (a) Rojo, T.; Mesa, J. L.; Lago, J.; Bazán, B.; Pizarro, J. L.; Arriortua, M. I. *J. Mater. Chem.* **2009**, *19*, 3793. (b) Bazán, B.; Mesa, J. L.; Pizarro, J. L.; Arriortua, M. I.; Rojo, T. *Prog. Solid State Chem.* **2007**, 205−238.

(5) (a) Halder, G. J.; Chapman, K. W.; Neville, S. M.; Moubaraki, B.; Murray, K. S.; Letaed, J. F.; Kepert, C. J. *J. Am. Chem. Soc.* **2008**, *130*, 17552−17562. (b) Neville, S. M.; Halder, G. J.; Chapman, K. W.; Duriska, M. B.; Moubaraki, B.; Murray, K. S.; Kepert, C. J. *J. Am. Chem. Soc.* **2009**, *131*, 12106−12108. (c) Southon, P. D.; Liu, L.; Fellows, E. A.; Price, D. J.; Halder, G. J.; Chapman, K. W.; Moubaraki, B.; Murray, K. S.; Letard, J. F.; Kepert, C. J. *J. Am. Chem. Soc.* **2009**, *131*, 10998−11009. (d) Hurd, J. A.; Vaidhyanathan, R.; Thangadurai, V.; Ratcliffe, C. I.; Maudrakovski, I. L.; Shimizu, G. K. H. *Nat. Chem.* **2009**, *1*, 705−710. (e) Sadakiyo, M.; Yamada, T.; Kitagawa, H. *J. Am. Chem. Soc.* **2009**, *131*, 9906−9907. (f) Cui, H. B.; Wang, Z. M.; Takahashi, K.; Okano, Y.; Kobayachi, H.; Kobayashi, A. *J. Am. Chem. Soc.* **2006**, *128*, 15074−15075. (g) Orive, J.; Mesa, J. L.; Balda, R.; Fernández, J.; Rodríguez-Fernández, J.; Rojo, T.; Arriortua, M. I. *Inorg. Chem.* **2011**, *50*, 12463−12476.

(6) Lin, H.; Maggard, P. A. *Inorg. Chem.* **2008**, *47*, 8044−8052.

(7) Chernova, N. A.; Roppolo, M.; Dillonb, A. C.; Whittingham, M. S. *J. Mater. Chem.* **2009**, *19*, 2526−2552.

(8) (a) Lee, J.; Farha, O. K.; Roberts, J.; Scheidt, K. A.; Nguyen, S. T.; Hupp, J. T. *Chem. Soc. Rev.* **2009**, *28*, 1450−1459. (b) Rowsell, J. L.; Yaghi, O. M. *Angew. Chem., Int. Ed.* **2005**, *44*, 4670−4679. (c) Fang, Q.-R.; Zhu, G.-S.; Ji, Y.-Y.; Ye, J.-W.; Xue, M.; Yang, H.; Wang, Y.; Qiu, S.-L. *Angew. Chem., Int. Ed.* **2007**, *46*, 6638−6642.

(9) (a) Larrea, E. S.; Fernández de Luis, R.; Mesa, J. L.; Pizarro, J. L.; Urtiaga, M. K.; Rojo, T.; Arriortua, M. I. In *Coordination Polymers and Metal Organic Frameworks: Properties, Types and Applications*; Ortiz, O. L., Ramirez, L. D., Eds.; Nova Science Publisher Inc.: New York, 2012; Chapter 1, pp 1−58. (b) Tao, J.; Zhang, X. M.; Tong, M. L.; Chen, X. M. *Chem. Soc. Dalton Trans.* **2001**, 770−771. (c) Xiao, D.; Li, Y.; Wang, E.; Wang, S.; Hou, Y.; De, G.; Hu, C. *Inorg. Chem.* **2004**, *42*, 7652−7657. (d) Li, Y.; De, G.; Yuan, M.; Wang, E.; Huang, R.; Hu, C.; Hu, N.; Jia, H. *Chem. Soc. Dalton Trans.* **2003**, 331−334.

(10) (a) Schindler, M.; Hawthorne, F. C.; Baur, W. H. *Chem. Mater.* **2000**, *12*, 1248−1259. (b) Zavalij, P. Y.; Whittingham, M. S. *Acta Crystallogr.* **1999**, *B55*, 627−663. (c) Zhang, Y.; Warren, C. J.; Haushalter, R. C.; Clearfield, A.; Seo, D.-K.; Wanhgho, M. H. *Chem. Mater.* **1998**, *10*, 1059−1064. (d) Zhang, Y.; ÒConnor, C. J.; Haushalter, R. C.; Clearfield. *Inorg. Chem.* **1996**, *35*, 4950−4956.

(11) (a) Fernández de Luis, R.; Urtiaga, M. K.; Mesa, J. L.; Rojo, T.; Arriortua, M. I. *J. Alloys Compd.* **2008**, *480*, 54−56. (b) Schindler, M.; Hawthorne, F. C.; Baur, W. H. *Can. Mineral.* **2000**, *38*, 1443−1456. (c) Livaje. *J. Coord. Chem.* **1998**, *178*−*180*, 999−1018.

(12) (a) Larrea, E. S.; Mesa, J. L.; Pizarro, J. L.; Rodríguez Fernández, J.; Arriortua, M. I.; Rojo, T. *Eur. J. Inorg. Chem.* **2009**, 3607−3612. (b) Hagrman, P. J.; Zubieta, J. *Inorg. Chem.* **2001**, *40*, 2800−2496. (c) Fernández de Luis, R.; Mesa, J. L; Urtiaga, M. K.; Lezama, L.; Arriortua, M. I.; Rojo, T. *New. J. Chem.* **2008**, *32*, 1582−1589. (d) Fernández de Luis, R.; Urtiaga, M. K.; Mesa, J. L.; Aguayo, A. T.; Rojo, T.; Arriortua, M. I. *CrystEngComm* **2010**, *12*, 1880−1886. (e) Larrea, E. S. Doctoral thesis, *New Transition Metal Hybrid Vanadates. Hydrothermal Synthesis, Structural Study and of their Spectroscopic and Magnetic Properties*, Universidad del País Vasco (UPV/EHU), 2009 .(f) Fernández de Luis, R. Doctoral Thesis, *Auto-Ensamblaje de Vanadatos Heterometálicos Basados en RedesMetal Orgánicas con Ligandos Bipodales*, Universidad del País Vasco (UPV/EHU), 2009. (g) Calderón, A. Doctoral thesis, *Transformaciones estructurales en arquitecturas supramoleculares basadas en el ligando PDC*, Universidad del País Vasco (UPV/EHU), 2012.

(13) Fernández de Luis, R.; Mesa, J. L.; Urtiaga, M. K.; Rojo, T.; Arriortua, M. I. *Eur. J. Inorg. Chem.* **2009**, 4786−4794.

(14) Fernández de Luis, R.; Urtiaga, M. K.; Mesa, J. L.; Vidal, K.; Lezama, L.; Rojo, T.; Arriortua, M. I. *Chem. Mater.* **2010**, *22*, 5543−5553.

(15) (a) Fernández de Luis, R.; Mesa, J. L.; Urtiaga, M. K.; Larrea, E. S.; Rojo, T.; Arriortua, M. I. *Inorg. Chem.* **2012**, *51*, 2130−2139. (b) Fernández de Luis, R.; Urtiaga, M. K.; Mesa, J. L.; Aguayo, A. T.; Rojo, T.; Arriortua, M. I. *CrystEngComm* **2010**, *12*, 1880−1886.

(16) (a) Chen, C.-L.; Goforth, A. M.; Smith, M. D.; Su, C.-Y.; zur Loye, H.-C. *Angew. Chem., Int. Ed.* **2005**, *44*, 6673−6677. (b) Calderón-Casado, A.; Barandika, G.; Bazán, B.; Urtiaga, M.-K.; Arriortua, M. I. *CrystEngComm* **2010**, *12*, 1784−1789. (c) Rather, B.; Zaworotko, M. J. *Chem. Commun.* **2003**, 830−831. (d) Zeng, M.-H.; Feng, X.-L.; Chen, X.-M. *Dalton Trans.* **2004**, 2217−2223. (e) Halder, G. J.; Kepert, C. J. *J. Am. Chem. Soc.* **2005**, *127*, 7891−7900.

(17) (a) Horike, S.; Dincă, Tamaki, K.; Long, J. R. *J. Am. Chem. Soc.* **2008**, *130*, 5854−5855. (b) Hong, D.-Y.; Hwang, Y. K.; Serre, C.; Férey, G.; Chang, J.-S. *Adv. Funct. Mater.* **2009**, *19*, 1537−1552. (c) Hasegawa, S.; Horike, S.; Matsuda, R.; Furukawa, S.; Mochizuki, K.; Kinoshita, Y.; Kitagawa, S. *J. Am. Chem. Soc.* **2007**, *129*, 2607−2614. (d) Platero-Prats, A.; de la Peña-ÓShea, V.; Iglesias, M.; Snejko,

N.; Monge, A.; Gutíerrez-Puebla, E. *Chem. Cat. Chem.* **2010**, *2*, 147−149.
(18) Forster, P. M.; Cheethanm, A. K. *Top. Catal.* **2003**, *24*, 79.
(19) Larrea, E. S.; Mesa, J. L.; Pizarro, J. L.; Iglesias, M.; Rojo, T.; Arriortua, M. I. *Dalton Trans.* **2011**, *40*, 12690−12698.
(20) Yingua, W. *J. Appl. Crystallogr.* **1987**, *20*, 258−259.
(21) Altomare, A.; Cascarano, G.; Giacovazzo, C.; Guagliardi, A. *J. Appl. Crystallogr.* **1993**, *26*, 343−350.
(22) (a) *SHELX97, Programs for Crystal Structure Analysis*; Sheldrick, G. M. Institüt für Anorganische Chemie der Universität: Göttingen, Germany, 1998. (b) Altomare, A.; Cascarano, G.; Giacovazzo, C.; Guagliardi, A. *J. Appl. Crystallogr.* **1993**, *26*, 343−350.
(23) Watkin, D. *Acta Crystallogr. A* **1994**, *50*, 411−437.
(24) (a) Fernández de Luis, R.; Urtiaga, M. K.; Mesa, J. L.; Orive Gomez de Segura, J.; Rojo, T.; Arriortua, M. I. *CrystEngComm* **2011**, *13*, 6488−6498. (b) Harada, J.; Keiichiro, O. *Chem. Soc. Rev.* **2009**, *38*, 2244−2252.
(25) (a) Liu, S.; Xie, L.; Gao, B.; Zhang, C.; Sun, C.; Li, D.; Su, Z. *Chem. Commun.* **2005**, 5023−5024. (b) Zhang, C.-D.; Liu, S.-X.; Gao, B.; Sun, C.-Y.; Xie, L.-H.; Yu, M.; Peng, J. *Polyhedron* **2007**, *26*, 1514−1522. (c) Dong, B.; Gómez-García, C. J.; Peng, J.; Benmansour, S.; Kong, Y. *J. Mol. Struct.* **2007**, *827*, 50−55. (d) Wang, X.-Y.; Wang, Z.-M.; Gao, S. *Chem. Commun.* **2007**, 1127−1129.
(26) (a) Li, X. L.; Sun, D.; Wang, Y.; Li, X.; Hong, M. *Cryst. Growth Des* **2004**, *4*, 775−780. (b) Marin, G.; Tudor, V.; Kravtsov, V. Ch.; Schmidtmann, M.; Simonov, Y. A.; Müller, A.; Andruh, M. *Cryst. Growth Des.* **2005**, *5*, 279−282. (c) Ma, C.; Chen, C.; Liu, Q.; Chen, F.; Liao, D.; Li, L.; Sun, L.; Eur, J. *Inorg. Chem.* **2004**, 3319−3325. (d) Luo, J.; Hong, M.; Wang, R.; Cao, R.; Han, L.; Yuan, D.; Lin, Z.; Zou, Y. *Inorg. Chem.* **2003**, *42*, 4486−4488.
(27) Fernández de Luis, R.; Urtiaga, M. K.; Mesa, J. L.; Arriortua, M. I. *Acta Crystallogr.* **2010**, *E66*, m323−m324.
(28) Aldous, D. W.; Goff, R. J.; Attfield, J. P.; Ligthfoot, P. *Inorg. Chem.* **2007**, *46*, 1277−1282.
(29) (a) CSD, Allen, F. H.; Kennard, O. *Chem. Des. Autom. News*, **1993**, *8*, 1, updated Aug. 2008, v. 5.29. (b) Allen, F. H.; Motherwell, W. D. S. *Acta Crystallogr., Sect. B: Struct. Sci.* **2002**, *B58*, 407−422.
(30) The search of hybrid vanadates containing Bpe guest molecules was done in the CSD database. The search was done imposing the existence of pyridil ring in their crystal structures. The composition was restricted to V, O, C, H, and N containing compounds, allowing also the presence of other atoms in the crystal structures. The 1280 compounds matching these criteria were carefully checked.
(31) Steiner, T. *Angew. Chem., Int. Ed.* **2002**, *41*, 48−76.
(32) http://www.topos.ssu.samara.ru; Blatov, A. V. *IUCr Comp. Comm. Newslett.* **2006**, *7*, 4−7.
(33) (a) Larrea, E. S.; Mesa, J. L.; Pizarro, J. L.; Arriortua, M. I.; Rojo, T. *J. Solid State Chem.* **2007**, *180*, 1149−1157.
(34) (a) Frost, R. L.; Erickson, K. L.; Weier, M. L.; Carmody, O. *Spectrochim. Acta* **2005**, *A61*, 829−834. (b) Watanabe, H.; Okamoto, Y.; Furuya, K.; Sakamoto, A.; Tasumi, M. *J. Phys. Chem. A* **2002**, *106*, 3318−3324. (c) Furuya, K.; Kawato, K.; Yokoyama, H.; Sakamoto, A.; Tasumi, H. *J. Phys. Chem. A* **2003**, *107*, 8251−8258. (d) Zhuang, Z.; Cheng, J.; Jia, H.; Zeng, J.; Han, X.; Zhao, B.; Zhang, H.; Zhang, G.; Zhao, W. *Vib. Spectr.* **2007**, *14*, 306−312. (e) Zubkov, V. G.; Surat, L. L.; Tyutyunnik, A. P.; Berger, I. F.; Tarakina, N. V.; Slobodin, B. V.; Kuznetsov, M. V.; Denisova, T. A.; Zhuravlev, N. A.; Perelyaeva, L. A.; Baklanova, I. V.; Shein, I. R.; Ivanovskii, A. L. *Phys, Rev.* **2008**, *B77*, 174113−1−174113−14. (f) Frost, R. L.; Erickson, K. L.; Weier, M. L. *Spectr. Acta A* **2004**, *60*, 2419−2423. (g) Frost, R. L.; Kristy, L.; Weier, M. L.; Cardomy, O. *Spectr. Acta A* **2005**, 829−834.
(35) Nakamoto, K. *Infrared Spectra of Inorganic and Coordination Compounds*; Wiley: New York, 1986.
(36) (a) Lever, A. B. P. *Inorganic Electronic Spectroscopy*; Elsevier Science Publichers B. V.: Amsterdam, Netherlands, 1984. (b) Sugano, T. Y. *J. Phys. Soc. Jpn.* **1954**, *9*, 753−766.
(37) Carlin, R. L. *Magnetochemistry*; Springer-Verlag: Berlin, Germany, 1986.
(38) Tietze, L. F.; Beifuss, U. In *Comprehensive Organic Synthesis*; Barry, M. T.; Ian, F., Eds.; Pergamon: Oxford, 1991.
(39) Cho, W. K.; Lee, J. K.; Kang, S. M.; Chi, Y. S.; Lee, H.-S.; Choi, I. S. *Chem.—Eur. J.* **2007**, *13*, 6351−6358.